Desalination and Water Treatment
www.deswater.com

doi: 10.1080/19443994.2014.989912

57 (2016) 6001–6006
March

Taylor & Francis
Taylor & Francis Group

Thermodynamic and kinetic study of $CaCO_3$ precipitation threshold

Raghda Hamdi[a], Marwa Khawari[a], Franck Hui[b], Mohamed Tlili[a,*]

[a]*Laboratoire de Traitement des Eaux Naturelles, Centre des Recherches et Technologies des Eaux, Technopole Borj Cédria, BP 273, Soliman 8020, Tunisia, Tel. +216 79 325 044; emails: hamdi.raghda@gmail.com (R. Hamdi), khawari.marwa@gmail.com (M. Khawari), mohamed.tlili@certe.rnrt.tn (M. Tlili)*

[b]*Laboratoire Interfaces et Systèmes Electrochimiques, UPR 15-CNRS, Université Paris VI, 4 Place Jussieu - Paris, France, Tel. +33 1 44 27 44 25; email: franck.hui@upmc.fr*

Received 12 February 2014; Accepted 11 November 2014

ABSTRACT

Calcium carbonate is one of the most sparingly soluble salts among those forming the scale. As its solubility is dependent on CO_2 and then pH, natural water exploitation equipment such as process, drinking or irrigation systems are often faced with a serious scaling problem. Having as an objective to control the scale formation, this present work aims at studying the $CaCO_3$ precipitation threshold using the classic fast controlled precipitation method. Studied solutions to be used are calco-carbonic waters ($[Ca(HCO_3)_2] = 0.4\ g\ L^{-1}$). Obvious results show that $CaCO_3$ precipitation threshold occurs at higher nucleation time and lower supersaturation coefficient with lower temperature, stirring speed and dissolved CO_2 degasification rate. The probability of $CaCO_3$ heterogeneous precipitation has increased with low stirring speed, low dissolved CO_2 degasification rate and low temperature.

Keywords: Calcium carbonate; Stirring speed; Dissolved CO_2; Temperature

1. Introduction

Calcium carbonate ($CaCO_3$) is a ubiquitous mineral in the environment. It precipitates into two classes: Hydrated forms: (Amorphous, monohydrate and hexahydrate $CaCO_3$) and anhydrous polymorphs: (Calcite, aragonite and vaterite). According to the Ostwald's step rule [1,2], several authors [3,4] have shown that one of the hydrated $CaCO_3$ variety precipitates at first and subsequently get transformed into a more stable one after several dehydration reactions, which is anhydrous polymorphs. The anhydrous calcite variety, which crystallizes in the rhombohedra shape, is thermodynamically the most stable one. This explains its predominance in the scale composition found in natural water systems. Its formation causes numerous technical and economical problems; from obstruction of pipes and seizure of valves to the fouling of desalination membranes [5–7].

To investigate the scaling formation mechanisms, various electrochemical and non-electrochemical methods were developed [8]. Numerous works using these methods have shown that $CaCO_3$ crystallization starts at a higher supersaturation level [9]. However, at industrial scale much lower values were recorded in incrusted circuits. So, to improve the reproduction of

*Corresponding author.

Presented at the 3rd Annual International Conference on Water (CI.EAU 2013), 18–20 November 2013, Algiers, Algeria

the scaling phenomenon in drinking water systems at a laboratory scale, the choice of the precipitation method is of great importance.

Considering that $CaCO_3$ scale crystallization is caused mainly by the displacement of the calco-carbonic equilibrium which is caused by dissolved-CO_2 degassing, the fast controlled precipitation (FCP) method [10,11] can be considered as the most appropriate technique. In fact, it has a great advantage in controlling the CO_2 degasification rate and the hydrodynamic of the solution, which are considered as the main parameters influencing the scaling of natural water circuits.

Because of its importance in the scaling phenomenon control, the nucleation process of $CaCO_3$ has been the subject of numerous investigations [12–14]. This present study is an attempt to understand the effect of several parameters: Hydrodynamic conditions, dissolved-CO_2 degasification rate and temperature on $CaCO_3$ nucleation threshold.

2. Material and methods

2.1. Water preparation

In order to avoid any side effects by foreign ions, calco-carbonic pure water (CCPW) is used. It was prepared by dissolving $0.4\,g\,L^{-1}$ reagent grade $CaCO_3$ in distilled water under CO_2 bubbling according to:

$$CaCO_3 + CO_2 + H_2O \rightarrow Ca^{2+} + 2HCO_3^-$$

The water pH resulting from this preparation was about 5.7.

For all experiments, the initial pH value was adjusted to 5.9, corresponding to a carbonate concentration of $[CO_3^{2-}] = 4.59\ 10^{-7}\,mol\,L^{-1}$ and a supersaturation coefficient of $\Omega = 0.25$ determined by using Eq. (1), to maintain the synthetic solution undersaturated.

$$\Omega_{CaCO_3} = \frac{[Ca^{2+}] \cdot [CO_3^{2-}] \cdot \gamma_{Ca^{2+}} \cdot \gamma_{CO_3^{2-}}}{K_s(calcite)} \quad (1)$$

where γ_i, [i] and K_s (calcite) are the activity coefficients, the ions concentrations and the calcite solubility product, respectively.

2.2. The FCP set up

The experimental set up of the FCP method was given in Fig. 1. A volume $V = 500\,mL$ of CCPW was placed in a polytetrafluoroethylene cell and immersed in a thermostatic water bath to maintain the temperature at 30°C. The solution was stirred at 800 rpm using a magnetic stirrer to accelerate the CO_2 degassing. During the FCP test the pH and the resistivity of the solution were continuously measured every two min, by a pH-meter (Hanna HI 110), and by a conductivity-meter (Meter Lab CDM 210). Calcium ion concentration was determined by EDTA complexometry titration.

2.3. The weight method

At the end of each FCP test, the full volume is filtered with a 0.45 μm pore size cellulose nitrate membrane to separate and to weigh the $CaCO_3$ mass m_b formed in the bulk of the solution by homogeneous precipitation. After measuring the calcium ions remaining in the solution, the total precipitated $CaCO_3 m_t$ was determined. The mass of $CaCO_3 m_w$ deposited on the cell wall by heterogeneous precipitation is deduced from the values of m_b and $[Ca^{2+}]$ [14].

The precipitation percentage was determined as follow:

$$\%_{hete} = \frac{m_w}{m_t} \times 100 = \frac{m_t - m_b}{m_t} \times 100 \quad (2)$$

3. Theory

The FCP method consists in the degassing of dissolved carbon dioxide ($CO_{2\ dissolved}$) from water by magnetic stirring, according to the following reaction:

$$CO_{2\ dissolved} \leftrightarrow CO_{2\ atmospheric}$$

Through this method, the nucleation and the growth of $CaCO_3$ are initiated in a similar way to a natural scaling phenomenon [8].

As the $CO_{2\ dissolved}$ degasses, the OH^-concentration increases, so the pH values increase and the supersaturation coefficient (Ω) begins to increase as well, according to:

$$HCO_3^- \leftrightarrow CO_{2\ dissolved} + OH^-$$

The reaction between OH^- ions and HCO_3^- ions can accelerate the germination and the growth of $CaCO_3$ and results in CO_3^{2-} ions according to:

$$HCO_3^- + OH^- \leftrightarrow CO_3^{2-} + H_2O$$

As the quantity of $CO_{2\ dissolved}$ decreases H^+ concentration increases and pH values decrease. Hence, the

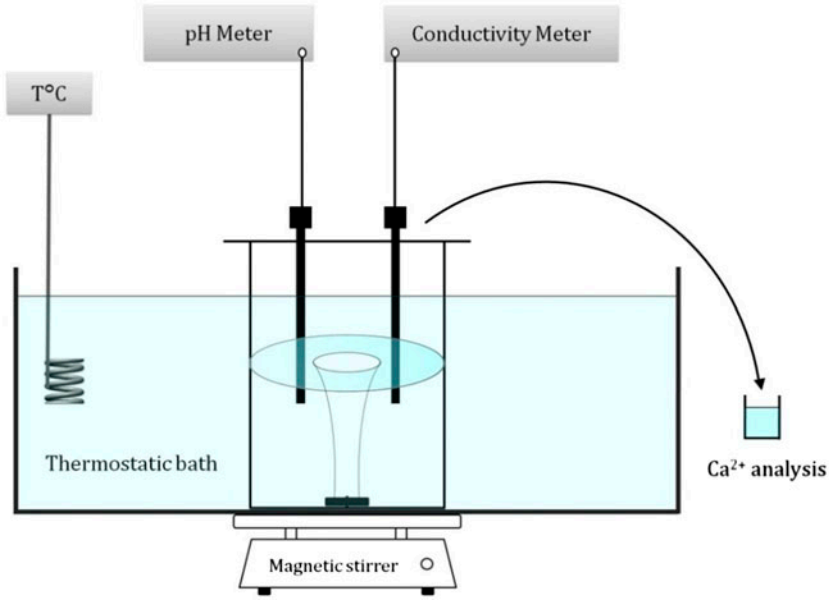

Fig. 1. The FCP experimental set up.

nucleation takes place, according to the following reaction:

$$CO_3^{2-} + Ca^{2+} \leftrightarrow CaCO_3 \downarrow$$

Finally, the temporal pH values become stable after reaching the dynamic equilibriums of both $CaCO_3$ nucleation and $CO_{2\ dissolved}$ degassing speed.

In Fig. 2 are reported experimental measurements of pH and resistivity vs. time of the CCPW solution during the precipitation process. In this experiment, the water hardness is 0.4 g L^{-1}, the temperature is 30°C and the stirring speed is 800 rpm. This figure highlights the frontier between three precipitation zones:

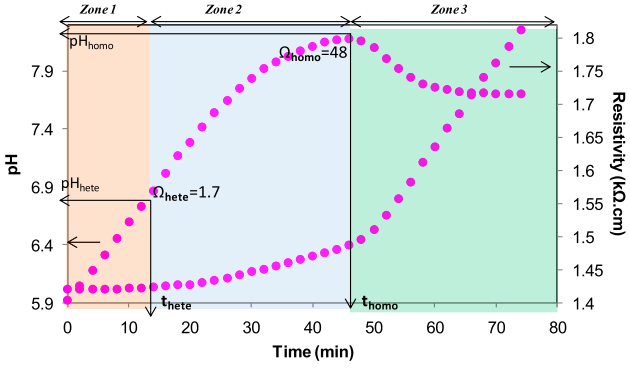

Fig. 2. Example of a FCP test with CCPW 0.4 g L^{-1}, at 30°C and at 800 rpm.

(1) Zone 1: where pH increases and resistivity is roughly constant from the precipitation experience onset up to 13 min. This means that the concentration of ions in the solution does not vary significantly and no precipitation occurred in the solution.
(2) Zone 2: where resistivity increases slowly and linearly. Furthermore, after reaching pH_{hete} at t_{hete}, the related pH values keep on increasing. Nucleation onset is possible. However, it's not easy to detect it. The first colloidal $CaCO_3$ nuclei appear in nanometric size and can adhere to the cell wall. In this case, the nucleation is heterogeneous.
(3) Zone 3: where resistivity continues to increase. The precipitation starts when the slope of resistivity–time curve changes. After reaching the $CaCO_3$ precipitation threshold at t_{homo} and pH_{homo}, a significant drop in pH is observed. $CaCO_3$ nuclei begin to be produced in the solution. Thus, the nucleation is homogeneous and a white suspension appears in the whole solution. Precipitation is rapid and followed by a growth phase.

4. Results and discussion

4.1. Effect of hydrodynamic conditions

The influence of hydrodynamic conditions on the precipitation threshold is studied by varying the

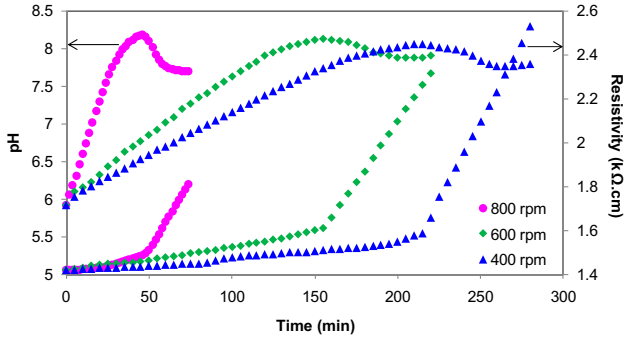

Fig. 3. Influence of stirring speed on precipitation threshold at 30 °C and CCPW 0.4 g L^{-1}.

stirring speed from 400 to 800 rpm. In Fig. 3 are reported experimental measurements of pH and resistivity vs. time of CCPW solution during the precipitation process. This figure shows that the time of the two nucleation decreases as stirring speed increases (Table 1).

Indeed, the acceleration of the metastable state breakdown, which corresponds to homogeneous precipitation, is attributed by Gal et al. [4] to the increased frequency with which precursors meet, and/or to the local heating caused by the friction of the magnetic stirrer, which accelerates the dehydration reactions of precursors in order to form other solids.

As shown in Table 1 and for the two nucleation thresholds, the time is roughly multiplied by 5 when stirring speed increases from 400 to 800 rpm. The heterogeneous nucleation threshold is always reached at Ω values ranging between 1 and 2. By contrast the homogeneous threshold is reached at low supersaturation coefficient when stirring speed decreases ($\Omega_{400rpm} = 35$; $\Omega_{800rpm} = 48$). Moreover, as shown in Table 1, stirring speed affects the adherence of scale on the cell wall. In fact, the heterogeneous precipitation percentage increases from 45 to 81% as stirring speed decreases from 800 to 400 rpm. These experimental data put to evidence that decreasing stirring speed promotes preferentially the heterogeneous precipitation of $CaCO_3$ detrimentally to the scaling in the bulk solution. In fact, nuclei can spend more time with low size, thus promoting its adsorption on cell walls at lower stirring speeds.

In order to study the influence of stirring speed on $CaCO_3$ precipitation threshold according to the solution saturation state, some modifications were made to the FCP method. At the beginning of this study, the solution was brought to the required pH, which is equal to 7.5, by magnetic stirring. The cell was then closed hermetically in order to limit CO_2 transfers between liquid and gaseous phases.

In Fig. 4 are reported experimental measurements of pH and resistivity vs. time of CCPW solution, during the precipitation process in order to study the stirring speed effect according to the solution saturation state.

Fig. 4 shows that at the same water hardness level and temperature, the $CaCO_3$ precipitation is possible at low pH values and consequently at low supersaturation coefficients. In fact at 800 rpm, $\Omega_{precipitation}$ decreases from 48 to 20 after closing the cell. As well as at 400 rpm, $\Omega_{precipitation}$ decreases from 36 to 24. Moreover, the massive $CaCO_3$ precipitation requires longer time to occur when supersaturation coefficients are low. Indeed at 800 rpm, the precipitation time of opened and closed cells were 46 and 95 min, respectively. As a result, precipitation was delayed by 49 min. Besides at 400 rpm, the precipitation time of opened and closed cells were 215 and 420 min, respectively. The retarding time of precipitation was 205 min.

4.2. Effect of dissolved-CO_2 degasification rate

The influence of dissolved-CO_2 degasification rate on the precipitation threshold was studied by varying the surface air–water contact from 2 to 102 mm^2. In order to study the influence of the surface air–water contact, we used a pierced cell cover. Holes in the cell cover are of different diameters. To control the surface contact, one or more of these holes were closed hermitically in order to limit CO_2 transfer between liquid and gaseous phases.

In Fig. 5 are reported experimental measurements of pH and resistivity vs. time of CCPW during the precipitation process. This figure shows that the metastable state breakdown, which corresponds to the massive homogeneous precipitation, requires longer time when the surface air–water contact decreases.

Table 1
Nucleation time, supersaturation coefficients and heterogeneous precipitation percentage as a function of stirring speed

Stirring speed (rpm)	t_{hete} (min)	Ω_{hete}	t_{homo} (min)	Ω_{homo}	$\%_{hete}$
400	50	1.2	215	35	81
600	35	1.3	155	41	60
800	12	1.7	46	48	45

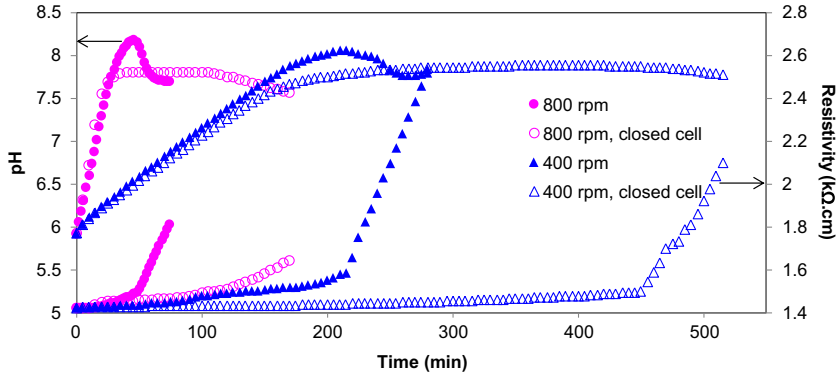

Fig. 4. Influence of stirring speed according to the solution saturation state at 30°C and CCPW 0.4 g L^{-1}.

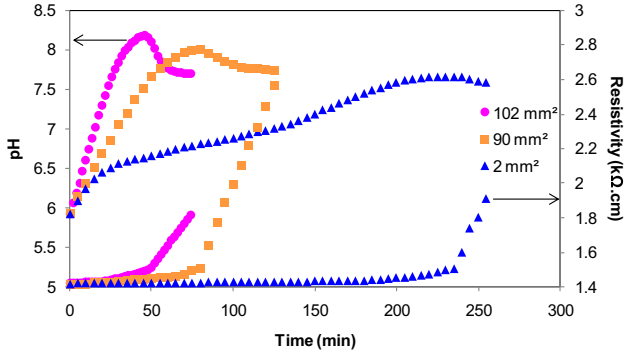

Fig. 5. Influence of surface air–water contact on precipitation threshold at 800 rpm, 30°C and CCPW 0.4 g L^{-1}.

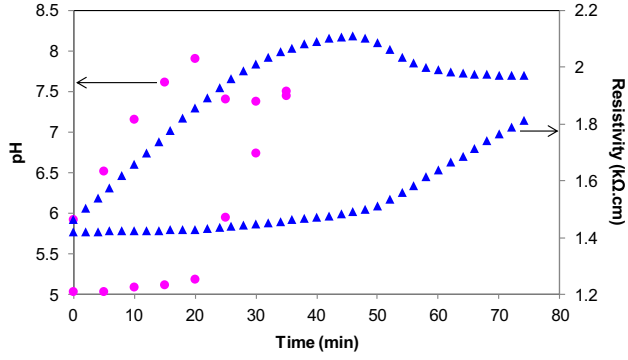

Fig. 6. Influence of temperature on precipitation threshold at 800 rpm and CCPW 0.4 g L^{-1}.

As seen in Table 2, t_{homo} increases from 46 to 235 min when surface air–water contact decreases from 102 to 2 mm^2. The resistivity-time curves plotted in Fig. 5 reveal that the distinction between the two zones 1 and 2 becomes more difficult after decreasing the surface air–water contact. In fact the resistivity increases with the same slope until it reaches the homogeneous nucleation threshold. Besides, in the pre-nucleation zone the slope of pH-time curves decreases gradually as surface air–water contact decreases. In fact, the rate of dissolved CO_2 degasification slows down as surface air–water contact decreases. Besides, it is commonly known that a reduction of dissolved CO_2 is followed by a rise of pH. Hence, the variation of pH-time curves slope decreases as dissolved CO_2 degasification rate decreases as well as surface air–water contact decreases. This rate reduction reduces the width of the metastable domain and favours the incrustation of the precipitate on the cell wall. Indeed the homogeneous threshold is reached at $\Omega = 14$ for a surface of 2 mm^2 whereas it is reached at $\Omega = 48$ for 102 mm^2 (Table 2). Moreover, the heterogeneous precipitation percentage calculated in Table 2 shows that the $CaCO_3$ wall adherence is favoured by the low dissolved CO_2 degasification rate and also by the low nucleation threshold.

Table 2
Nucleation time, supersaturation coefficients and heterogeneous precipitation percentage as a function of surface air–water contact

Surface air–water contact (mm^2)	t_{hete} (min)	Ω_{hete}	t_{homo} (min)	Ω_{homo}	$\%_{hete}$
102	12	1.7	46	48	45
90	20	1.5	80	31	56
2	–	–	235	14	60

Table 3
Nucleation time, supersaturation coefficients and heterogeneous precipitation percentage as a function of temperature

Temperature (°C)	t_{hete} (min)	Ω_{hete}	t_{homo} (min)	Ω_{homo}	$\%_{hete}$
30	12	1.7	46	48	45
50	5	2	20	49	30

4.3. Effect of temperature

The temperature is a major factor which affects the nucleation kinetics. Theoretically, the nucleation time is defined as follow [15]:

$$\log t_{N\ theoretical} = A + \frac{B}{\log^2 \Omega} \quad (3)$$

where A is a constant, $B \propto \sigma/T$ where σ is the interfacial tension and T is the temperature and Ω is the supersaturation coefficient: if the temperature increases, the nucleation time decreases.

In Fig. 6 are reported experimental measurements of pH and resistivity vs. time of CCPW during the precipitation process. As expected, the curves plotted in Fig. 6 show that the higher the temperature is the shorter the nucleation time is.

As shown in Table 3, when temperature increases from 30 to 50°C, t_{homo} decreases from 46 to 30 min whereas the supersaturation coefficient remains roughly constant, since Ω_{homo} is 48 at 30°C and is 49 at 50°C. Moreover, Table 3 shows that $\%_{hete}$ decreases from 45 to 30% as temperature increases from 30 to 50°C. Consequently, the temperature favors the formation of $CaCO_3$ nucleus in the bulk of the solution and influences both the kinetic and thermodynamic of the precipitation.

5. Conclusion

This paper investigates the precipitation threshold of $CaCO_3$ with FCP method in different experimental conditions to inhibit $CaCO_3$ formation. The results can be summarized as follows:

(1) The FCP tests show that the nucleation time was shorter and the supersaturation coefficient was higher for high agitation speed (800 rpm), high temperature (50°C), and large surface air–water contact (102 mm^2).
(2) The probability of $CaCO_3$ formed nucleus adhesion on the cell walls has increased by low stirring speed, low dissolved CO_2 degasification rate and low temperature.
(3) The solution saturation state has decreased and the nucleation time was highly delayed after the modifications made to the FCP method. As a consequence, it is better to work with a closed cell than with an opened one.

References

[1] O. Söhnel, J. Garside, Precipitation, Butterworth-Heinemann, Oxford, 1992.
[2] W.Z. Ostwald, Studien über die bildung und umwandlung fester körper (studies on the formation and transformation of solids), Phys. Chem. 22 (1879) 289–330.
[3] M.M. Tlili, M. Ben Amor, C. Gabrielli, S. Joiret, G. Maurin, On the initial stages of calcium carbonate precipitation, Eur. J. Water Qual. 37 (2006) 89–108.
[4] J.Y. Gal, Y. Fovet, N. Gache, Mechanisms of scale formation and carbon dioxide partial pressure influence. Part I. Elaboration of an experimental method and a scaling model, Water Res. 36 (2002) 755–763.
[5] L. Legrand, P. Leroy, Prevention of Corrosion and Scaling in Water Supply Systems, E. Horwood, New York, NY, 1990.
[6] T. Chen, A. Neville, M. Yuan, Calcium carbonate scale formation—Assessing the initial stages of precipitation and deposition, J. Petrol. Sci. Eng. 46 (2005) 185–194.
[7] D. Gebauer, A. Völkel, H. Cölfen, Stable prenucleation calcium carbonate clusters, Science 322 (2008) 1819–1822.
[8] F. Hui, J. Lédion, Evaluation methods for the scaling power of water, Eur. J. Water Qual. 33 (2002) 55–74.
[9] M.M. Tlili, M. Benamor, C. Gabrielli, H. Perrot, B. Tribollet, Influence of the interfacial pH on electrochemical $CaCO_3$ precipitation, J. Electrochem. Soc. 150 (2003) C765–C771.
[10] J. Lédion, B. François, J. Vienne, Characterization of the scaling properties of water by fast controlled precipitation test, Eur. J. Water Qual. 28 (1997) 15–35.
[11] G. Gauthier, Y. Chao, O. Horner, O. Alos-Ramos, F. Hui, J. Lédion, H. Perrot, Application of the fast controlled precipitation method to assess the scale-forming ability of raw river waters, Desalination 299 (2012) 89–95.
[12] W. Mejri, A. Korchef, M. Tlili, M. Ben Amor, Effects of temperature on precipitation kinetics and microstructure of calcium carbonate in the presence of magnesium and sulphate ions, Desalin. Water Treat. 52 (2014) 4863–4870.
[13] D. Liu, W. Dong, F. Li, F. Hui, J. Lédion, Comparative performance of polyepoxysuccinic acid and polyaspartic acid on scaling inhibition by static and rapid controlled precipitation methods, Desalination 304 (2012) 1–10.
[14] M. Ben Amor, D. Zgolli, M.M. Tlili, A.S. Manzola, Influence of water hardness, substrate nature and temperature on heterogeneous calcium carbonate nucleation, Desalination 166 (2004) 79–84.
[15] A.F. Hidalgo, C. Orr Jr., Homogeneous nucleation of sodium chloride solutions, Ind. Eng. Chem. Fund. 7 (1968) 79–83.